Science Arts & Métiers (SAM)

is an open access repository that collects the work of Arts et Métiers Institute of Technology researchers and makes it freely available over the web where possible.

This is an author-deposited version published in: https://sam.ensam.eu
Handle ID: .http://hdl.handle.net/10985/8524

To cite this version :

Sébastien VOISEMBERT, Alain RIWAN, Améziane AOUSSAT, Nazih MECHBAL - Design of a novel long-range inflatable robotic arm: Manufacturing and numerical evaluation of the joints and actuation - Journal of Mechanisms and Robotics - Vol. 5, n°4, p.9 - 2013

Any correspondence concerning this service should be sent to the repository Administrator : scienceouverte@ensam.eu

Arts et Métiers Institute of Technology

Design of a Novel Long-Range Inflatable Robotic Arm: Manufacturing and Numerical Evaluation of the Joints and Actuation.

Sébastien Voisembert

Interactive Robotics Laboratory

CEA-LIST, and PhD student at the LCPI, EA, AMPT

Paris 75013, France

e-mail: sebastien.voisembert@cea.fr

Nazih Mechbal

PIMM, UMR-CNRS, AMPT

Paris 75013, France

e-mail: Nazih.Mechbal@paris.ensam.fr

Alain Riwan

Interactive Robotics Laboratory

CEA, LIST

Fontenay aux Roses, F- 92265, France

e-mail: alain.riwan@cea.fr

Ameziane Aoussat

LCPI, Product Conception and Innovation Laboratory

EA, AMPT

Paris 75013, France

e-mail: Ameziane.AOUSSAT@ensam.eu

The aim of this paper is to present the design of a new long range robotic arm based on an inflatable structure. Inflatable robotics is on the horizon. It has potential for improved large payload-to-weight ratios, safe collision and inspection in areas inaccessible to human beings as in nuclear plants. The present robot is intended to operate inspection or maintenance missions in critical installation with taking care to not collide with its environment. It is made with innovative inflatable joints and an original actuation system. Prototypes of this inflatable manipulator were constructed using two different manufacturing procedures. Both were tested and numerically analyzed. The specific geometry of joints was studied and an analytical model for control purpose is proposed here

The experimentation results validated this new concept of robotic arm. Moreover, using LS-DYNA nonlinear dynamic finite element modeling we have analyzed the complete dynamical behavior of a joint. The simulations have given insight into understanding the joint bending process and have revealed guidance for optimizing the conception.

1 Introduction

Inflatable robots have become attractive because they can meet structural requirements for several expensive applications at a low cost. Moreover, their inherent abilities such as lightweight, large payload-to-weight ratios, and safe collision, have made them very appealing for specific manipulations as inspections operations in confined area or to operate in human environments. Nowadays, considerable effort is being devoted to the development and prototyping of inflatable manipulators. Several new robots and actuators built out of fabric and powered via pneumatics or hydraulics have been developed. The first proposed inflatable manipulators were high degrees of freedom trump-like manipulators. As an example, the Octarm [1] is a bio-mimetic manipulator composed of inflatable actuators. It can handle objects with any kind of shape thanks to its highly compliant pneumatic muscles. Other manipulators were designed in a lightweight purpose with inflatable links and classical revolute joints [2-4]. Sanan also created inflatable manipulators for safe interaction with humans [5, 6]. Indeed, as they are not made of metals or carbon fibers like other classical robots, accidental contacts with operators are no longer causes of injuries. Furthermore, they are low-cost, lightweight and easy to store when deflated.

One of the major challenges in robotics is the improvement of inspections operations in hazardous area using unmanned remote handling systems. Articulated arms could be used in this case to carry some diagnostic tools for the inspection tasks. These long reach multi-link carriers should be characterized by a large workspace and reduced mass. These serial tendon driven manipulators are mainly composed of a support base and a long range redundant serial arm made of links and joints. They are widely used for inspection tasks in hostile environment such as nuclear industry, where a lot of cells to be inspected are only accessible through a very narrow hole.

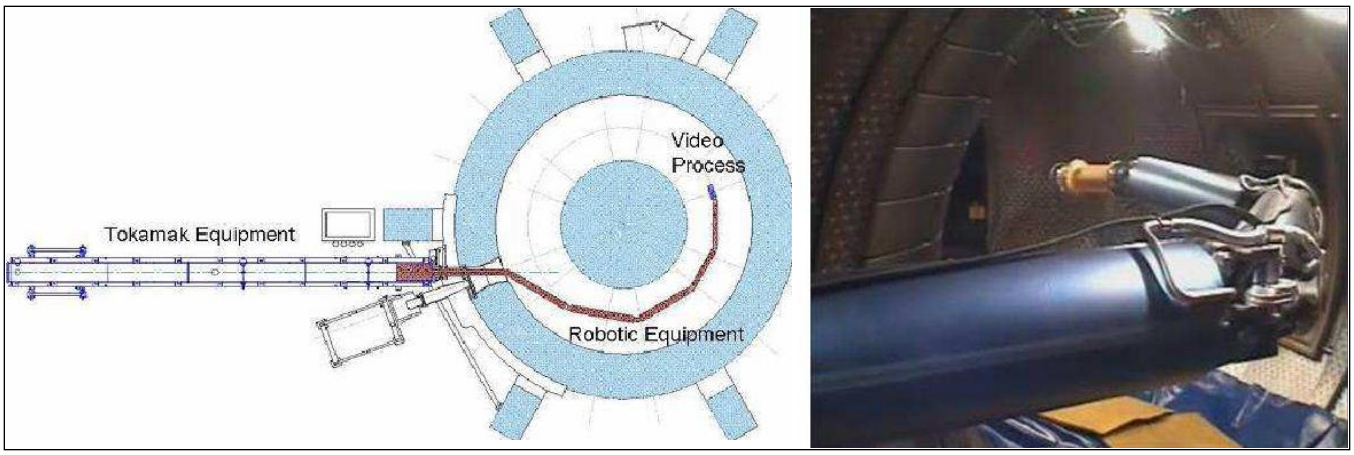

Fig. 1 : AIA robot into a full vessel demonstrator (scale 1) [7].

For example, in the case of maintenance operations in fusion reactors; particularly Plasma Facing Components viewing and leak testing inspections, the accessibility to the inspection area is only possible through some openings evenly distributed around the machine. Since 2005, the Interactive Robotics Laboratory of the CEA, the French Government Atomic Commission, has proposed and developed for the inspection of the vacuum vessel of Tokamak Fusion reactor Tore Supra and further ITER, a teleoperated arm named AIA (Articulated Inspection Arm). The AIA robot (Fig. 1) is an 8 *m* long multi-link carrier with payload up to 10 *kg* and a total weight of 150 *kg*. The polyarticulated arm can be introduced in the vessel through a small port of 250 *mm* diameter and should bear a 10^{-6} *Pa* vacuum and 150°*C* temperature [8]. On inspection mission the robot has to navigate around critical and fragile devices with taking care to not collide with them.

The arm should also have enough torque to carry its own weight plus the payload in cantilever mode and enough stiffness to minimize the deflection caused by the gravity. Moreover, for long reach we need to increase the number of joints and reduce the mass which therefore increases significantly the structural compliance. For a given material and with a constraint on the outer diameter, it can be shown that the deflection of a tube increases with its thickness.

In the Euler-Bernoulli beam theories, the deflection under its own weight of a cylindrical cantilever beam is given by:

$$Y = \frac{-g\rho L^4}{8E} \cdot \frac{S}{I} \tag{1}$$

Where Y denotes the deflection at the end of the beam, g is the gravity, ρ is the density of the material, L is the length of the beam, E is the Young modulus of the material, S is the cross section area of the beam and I is the second moment of area.

If we introduce t as the thickness of the beam, we have

$$\frac{S}{I} = \frac{2}{R^2} \cdot \frac{1}{1 + \left(1 - t/R\right)^2} \tag{2}$$

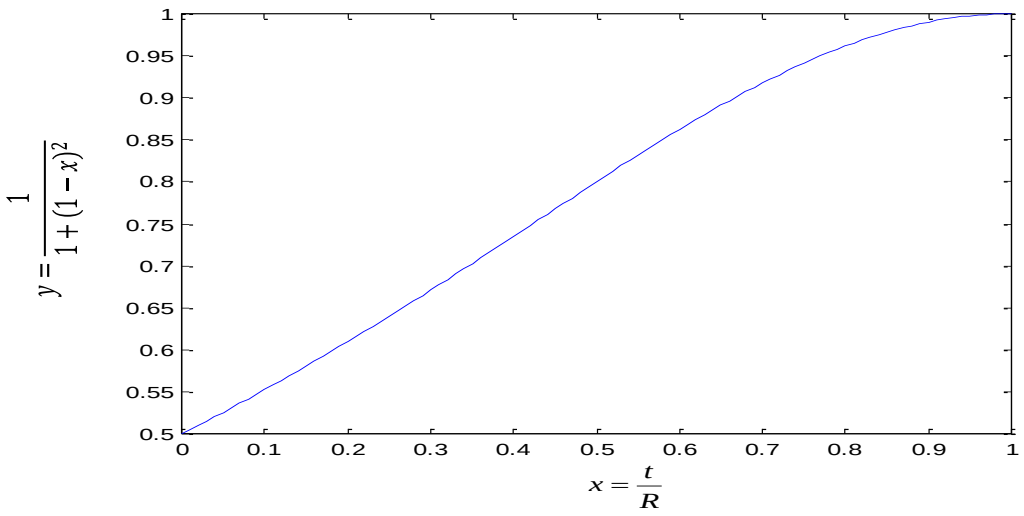

Fig. 2: Influence of the thickness ratio on the deflections of a cantilever beam submitted to its own weight.

As shown in Fig. 2, a small thickness reduces the deflection. Unfortunately, for thin wall structures, the compressive strength is limited by buckling. This example brought out the question of how to increase compressive strength without adding weight? A solution is given by the concept of tensegrity where some elements bear compressive stress while other bear tensile stresses.

Hence, the robot body can be designed to be made of a light membrane or fabric, which bears only tensile stresses and another material, could be used to bear compressive stresses. The evident cheapest and lightest material that comes up in mind, in order to bear compressive strengths is air. In fact, the gas can be compressed inside the structure and pre-stress it. As a result, the buckling appears only when the compressive stress overtakes the pre-stress. In this study, a challenging design issue is addressed to improve significantly the operational range of these robots. We present here an innovative design of long range robots, named LRIA (Long Rang Inflatable Arm). The concept of tensegrity is used to make significant improvements on the weight and the cost of the arm. The proposed structure has the same overall shape as a classic multi-link arm, *i.e.* an alternation of links and joints. However, it is made of non-stretch fabric tightly coated. The benefits of such a robot are straightforward and obvious. For a light payload, *i.e.* 1 *kg* (for example, the weight of an inspection camera), the arm can reach very important length. Furthermore, it is easily movable when deflated and the setup can be rapid. Moreover, these arms can be fabricated and deployed with a drastic reduction of the cost according to conventional long range robots as for example the AIA robots-like. In this paper, we present new features of design and modeling of such a robot. We used a one-axis rotational joint with toroïdal bending at constant volume [3]. It presents several benefits such as good stiffness in directions cross its rotation axis and low bending torque along its axis. This kind of joint was developed for spacesuits (Fig. 3) but with inner pressures lower than 30 *kPa*, whereas the minimum pressure needed by an inflated beam with the typical dimensions of a long range robot (10*m* long and 0.2*m* of diameter) that carries 1 *kg* is 130 *kPa*.

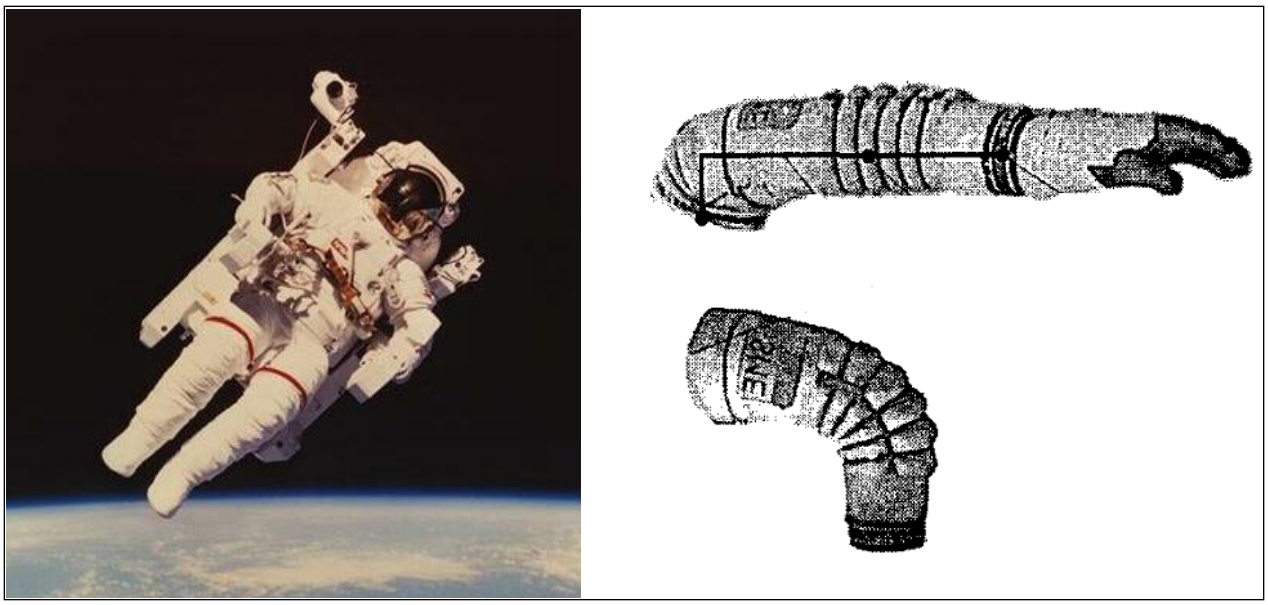

Fig. 3: Spacesuit joints are composed of bellows [9].

Based on these statements, we present in the sequel two new designs of a higher pressure inflated structure convenient for very long range robots. Both designs have been tested on prototypes but not on the same material because of realization convenience. Thus in order to compare them, a dedicated finite element model has been developed. The finite element approach is also chosen as a simulation and design tool because of its ease of modeling complex geometries and ability to provide visualization. To take into account large displacements and membrane inflation, simulations were conducted using the explicit code LS-DYNA® (by LSTC). The simulations have given insight into understanding the bending process and revealed guidance to optimize the design. For control purpose of the robot, a study of the geometrics and kinematics of the inflatable joints must be driven. Therefore we present in this paper a first analytical model-based design of an n-DOF serial inflatable robot.

The remainder of this paper is organized as follows: Section 2 presents the finite element modeling that is used in the new designs evaluation in Section 3, and Section 4 deals with the numerical optimization of the tendon driven actuation system. We conclude and present future works in Section 5.

2 Finite element study of the design

Explicit integration is often used for deployment simulations. It requires small time steps that are selected according to the complexity of the shape and the dynamics of the deployment. With the control volume (CV) approach available in LS-DYNA, the effect of inflation gas inertia is not directly included.

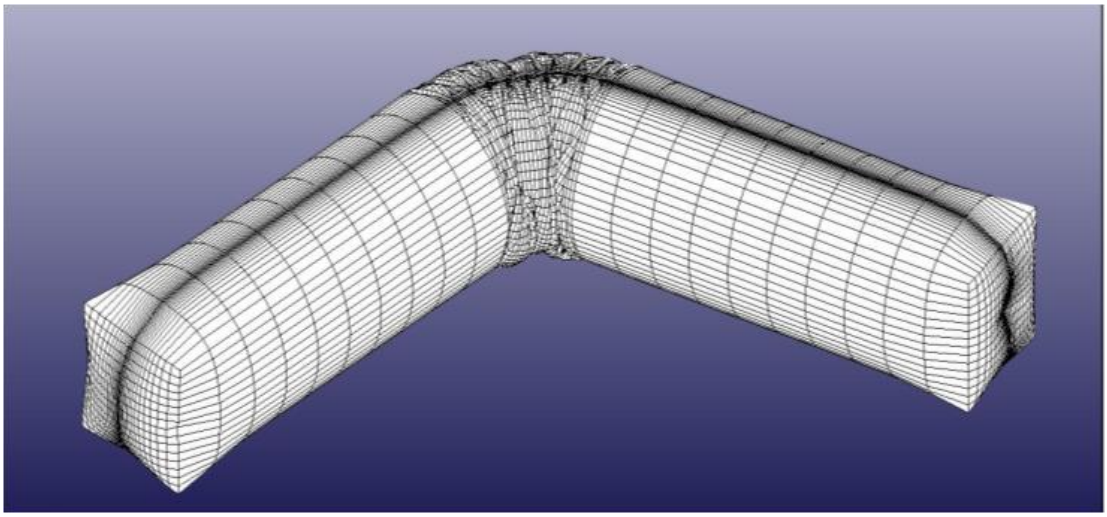

Fig. 4: Finite element model of two links and one central joint.

2.1 Presentation of the finite element model.

The finite element simulation aims at modeling accurately the shape of an inflatable arm according to our design. The objective is to predict numerically the behavior of a prototype after its inflation when submitted to actuation efforts. And more precisely, it aims at comparing the performances of two manufacturing procedures.

2.1.1 Simulation model

Finding the shape of an inflatable structure is now a solved problem but is still a large field of research for finite elements codes [10-17]. For examples, the form finding of inflated structures with very low shear modulus materials is still unsolved. An inflated membrane raises several other mechanical problems such as large displacement calculation of membrane elements with no stiffness in flexion and self-contact [18]. In order to take into account all the complexity of this problem we use membrane models and dedicated algorithms developed within the LS-DYNA® finite element code by LSTC.

Here a prototype composed of two links and one central joint is discretized by finite elements. The links are 50cm long and the joint has theoretical amplitude of 90°. All the parts have the same diameter of 200*mm* (see Fig. 4). The fabric is represented by the material model *MAT_FABRIC [19, 20], a four nodes element well adapted to airbags inflations. Buckling is well represented even with a coarse mech. The mechanical properties chosen are consistent with the Dyneema® fabric used for the prototypes. An orthotropic model is applied with 11 *GPa* in warp and weft directions, which coincides with the longitudinal and transverse direction of the prototype. The shear modulus should be based on the properties of the polyurethane bladder but compared to the young modulus of the fabric, the value is too low to be computed. The minimum computable value is used instead.

The joint allows a rotation motion thanks to the pleats. The pleats modeling will be described in the next parts. The seams are assumed to be non-stretched so they are represented by some fabric elements stiffer than the rest of the fabric. The scenario of the simulation is twofold: first the virtual prototype is inflated to a pressure of 0.1 *Mpa* in 0.5 *s* to get the proper initial inflated shape. This phase is short because the inflation is not important in the simulation. Then the pleats are created and a constant bending force between the extremities of the joint is applied by a muscle element *MAT_SPRING_MUSCLE [19, 20]. The muscle stands for the pulley blocks actuation system that will be presented in Section 4. It can be attached on several points of the joint to simulate different pulley blocks. This second phase is set to last 10 seconds in order to give enough time to the joint to bend. Gravity load is not applied.

2.1.2 Inflation model

The modeling treats the virtual prototype as a control volume, where the control surface is modeled by the fabric material. The expansion is considered adiabatic and the ideal gas law is used. Algorithms within the LS-DYNA® finite element code are based on an airbag inflation model developed by Wang and Nefske [21, 22]. During all the simulation, the pressure, the volume and the temperature are recorded.

2.1.3 Contact model

Due to the complex shape of the joint, a consistent simulation must take into account the self-contact of the fabric. Indeed, experimentations show that when inflated, the excess of fabric in the joint (due to the folds) leads to the apparition of unexpected pleats.

Three contact treatments exist in LS-DYNA but all of them consider that one of the surfaces involved in the contact is a master surface and the other the slave surface. The master surface is not deformed by the contact efforts whereas the slave surface does. The most common is the penalty method; it consists in detecting penetrating nodes or edges and to apply a repulsive effort normal to the surface. This effort is calculated according to the elastic law of a virtual spring placed between the surface and the penetrating node. The stiffness of the spring depends on the mechanical properties of each element, its stiffness, its size, its surface and its bulk modulus. The value is given by (3):

$$k_i = \frac{f_{si} K_i A_i}{V_i} \tag{3}$$

where k_i denotes the spring stiffness, f_{si} is an adjustment factor set to 1, K_i is the bulk modulus of the fabric, A_i is the surface of the penetrated element and V_i its volume. The second method is the kinematic constraint method. It does not allow penetration until there is a tension applied on the surface, the contact nodes are constrained by additional accelerations and velocities to stay on the contact surface. This way, the contact nodes follow the surface contact in its motion.

The distributed parameter method is the last one: it is the same as the second one except that half the mass of the slave nodes is distributed on the master surface. Nevertheless, only the penalty method is implanted for self-contact problem then this is the method used for our simulations.

Three friction models are available in LS-DYNA, the sliding only contact, static and dynamic friction and viscous friction.

Static and dynamic frictions are based on the model of Coulomb, with a smooth interpolation between the static and dynamic friction coefficient given by:

$$\mu = \mu_d + (\mu_s - \mu_d) e^{-carb|v|} \tag{4}$$

where μ denotes the coefficient of friction, μ_d is the dynamic coefficient of friction, μ_s is the static coefficient of friction, v the relative velocity of the surfaces and $carb$ is an arbitrary constant set by the user. The viscous damping is consistent with the Rayleigh model where the viscous damping matrix is given by multiplying the coefficient of viscous friction with the mass matrix.

In the simulations, only the Coulomb friction model is used. Two cases are performed in order to evaluate the effect of friction on the joint bending. In the first, the coefficients of friction are set to zero, and in the second, for simplicity, both static and dynamic coefficient of friction are set to the static coefficient of friction of the PVC (usual fabric coating) which value is 0.15.

2.1.4 Meshing

For all the following simulations, the meshing is composed of quadrangles. The link is similar to a simple inflatable beam which mechanical behavior is well known [23-26]. Then the meshing in the links is really coarse, elements are 50 *mm* long and 10 *mm* large. On the contrary, the meshing has been refined at the joint in order to represent accurately its behavior. Nevertheless, if the elements are too small, calculation time becomes unacceptable. This is a well-known problem of explicit finite element calculation. According to the Courant-Friedrichs-Lewy law [27], the time step cannot be smaller than the Courant time step which depends on the material stiffness and the size of the element. The meshing used is a compromise between a good accuracy and an acceptable time calculation. Furthermore, in order to simulate the orthotropic fabric, the elements are oriented along the longitudinal and the circumferential axis.

2.1.5 Validation

In order to validate the FE simulation, we have compared the deflections under vertical load of a real prototype with the deflections calculated by the modeling.

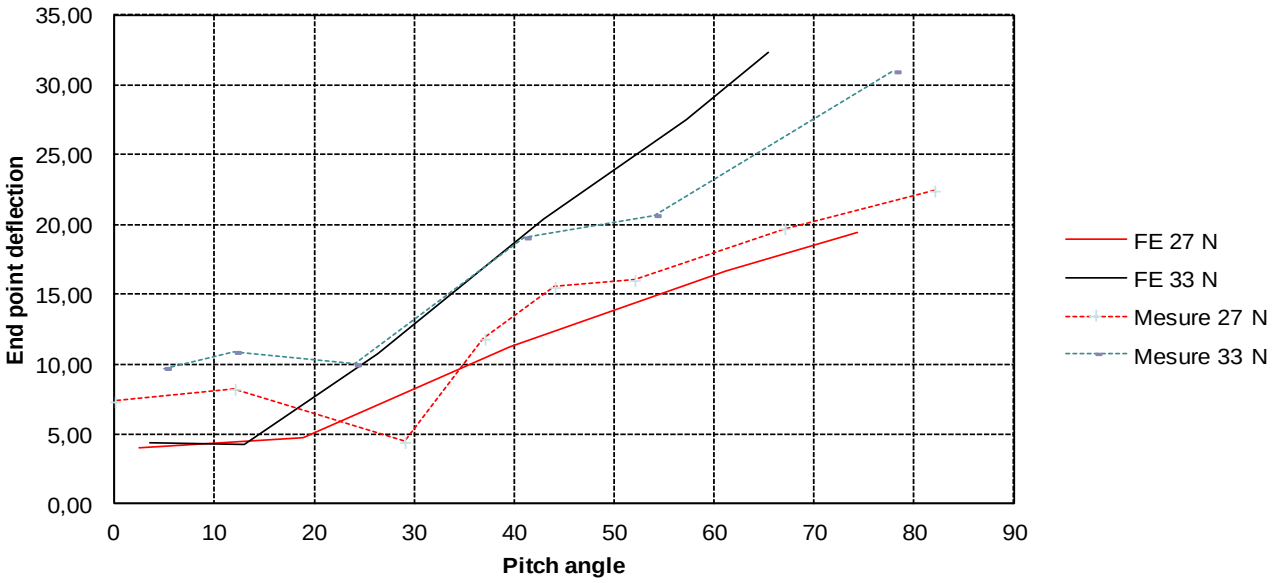

Fig. 5: End point deflections calculated with the FE model and compared with experimental values

The prototype is composed of two links and one vertical axis joint inflated at 45000 *Pa*. One of the links is constrained and loads of 27 and 33 *N* are applied at the end of the second link for different pitch angles. In Fig. 5, the measured and calculated deflections are compared. The differences between the reality and the model can be explained by the poor quality of the prototype used in this experiments and the inaccurate shear modulus value. Nevertheless, this modeling is accurate enough to represent the behavior of inflated joints and make qualitative deduction concerning the design.

3 New designs of the inflatable arm

3.1 Design of a joint.

Here a 90° amplitude joint is taken as a design example. The inflatable joint must be able to change shape from a cylinder to a quarter of a torus with no volume variation. Hence, one side of the cylinder must extend until taking a toroïdal shape. The simplest way to reach this ability is to attach 2 portions of a torus by their middle line (Fig. 6).

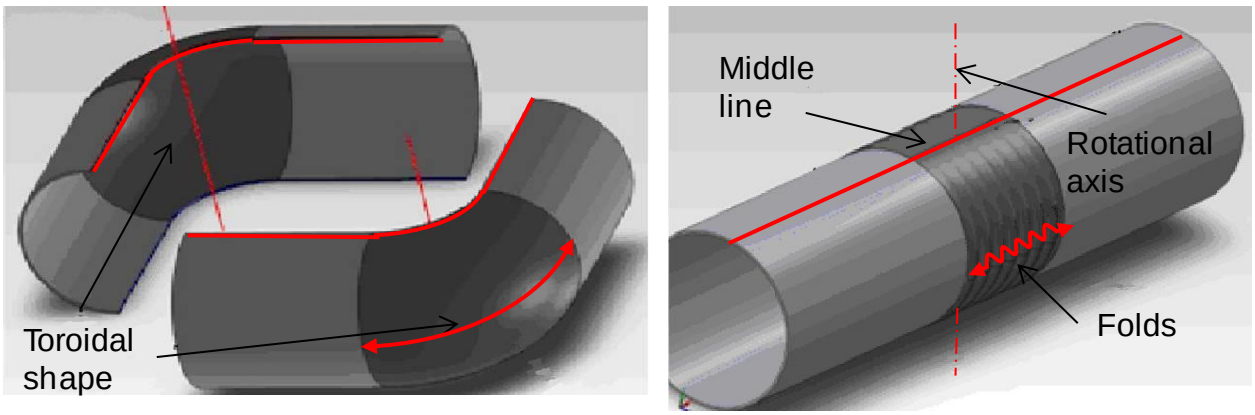

Fig. 6: Ideal shape of an inflatable joint.

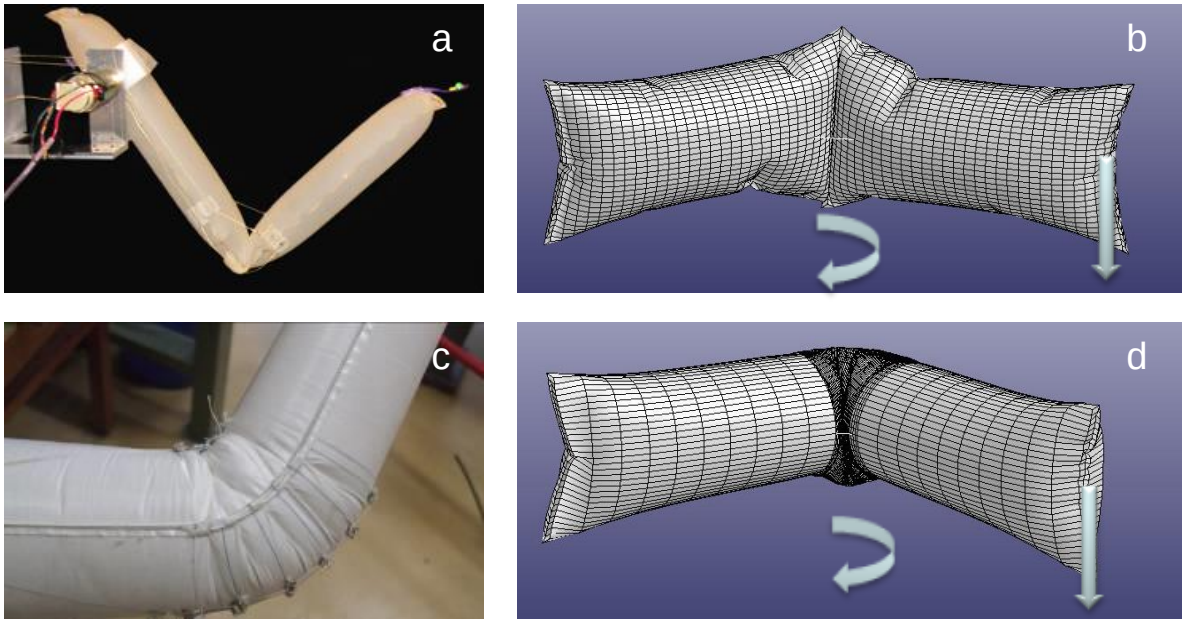

Fig. 7: Sanan's robot arm(a) and a simulated model (b). Our prototype with a Space-suit like inflatable joint (c) and a simulated model (d).

Unfortunately, this shape cannot be obtained from a 2 dimension fabric but can be approximated with a special confection. It consists in shortening the middle line of the joint by making pleats and sewing them together. Since the spatial conquest, this kind of joint has been used in space suits to allow astronauts moving in a suit stiffened by the internal pressure. However, this kind of joint has never been used in a robotic application. Sanan has proposed a simpler joint based on a section restriction and we have used a FE simulation to find out which joint best suits our long-range robot.

As our future robot is intended to work in the horizontal plane with gravitational loads in vertical plane, the joint we seek must be as compliant as possible along its rotational axis and as stiff as possible in cross directions. In the simulation, both designs are modeled and submitted to the same test: they are bent by a constant force of 90 *N* and a payload of 50 *N* is applied at the free extremity (Fig. 7). For our design, bellows are modelled by pleats on the flat fabric. Here the mechanical behaviour of both joints are compared *i.e.* the bending aptitude and the resistance to bending cross the rotation axis.

Compared to the Sanan's joint the bellow type joint exhibits twice the bending amplitude and is twice as stiff in flexion (Table1).

Table 1 :Comparative evaluation of the joints

Joint type	Max bending angle (°)	Deflection in cross direction (mm)
Space-suit joint	81	11
Section restriction	47	20

This fact confirms that keeping the cross section constant along the arm increases dramatically its performance. Therefore the bellow type joint is selected for the following work.

3.2 Practical realization

The two principal functions the arm envelope should provide are air tightness and mechanical resistance to stress. Air tightness can be ensured by an inner tube while the mechanical requirement may be met by an independent fabric. Nevertheless, assembling the fabric with a bladder may be difficult for a long robot arm. As a consequence, we propose to use a coated fabric to realise the robot. With this kind of fabric, both functions are fulfilled at the same time but the seams must be carefully over coated. In previous prototypes the pleats were sewed together but, with a coated fabric, this method is no longer valid because the seam must be planar in order to be over-coated. Basically, the purpose of the pleats is to shorten the middle line of the cylinder, but shortening this line may also be done without seams. Here, we propose and compare two manufacturing processes that allow building inflatable joints made of a tight coated fabric. Theoretically, both methods are effective but we have also tested their convenience and the actuation torque of the resulting joints with experiments and simulation.

3.2.1 Stop-pin based solution

The main difficulty is in the region where the length of the cylinder is shortened, all the tensions are concentrated and pull on the pleats, *i.e.* for $10^5 Pa$ in a 200 *mm* cylinder, the shortened lines (Fig. 8b) must bear a tension of 1570 *N*. Here, we propose an assembling method to realise pleats that can bear this tension. The idea is to constrain the pleats within a rigid shape. Thus, we have used stop-pins as intern and extern shapes (Fig. 8a). The intern stop-pin keeps the fabric inside another stop-pin which bears the tension. With this solution, the joints can be placed everywhere in the robot without seams. Furthermore, the joints are removable, which introduce modularity in the robot architecture.

Nevertheless, we have noted that intern stop-pins slowly slide out of the extern stop-pin until it is dangerously expelled by the fabric. This problem can be solved by replacing intern stop-pins by screws (Fig. 8c). The length L_g of the stop-pin is an important parameter, obviously, if the stop-pin is to short the fabric cannot bear the stress concentration; and if it is too long the joint bending is limited.

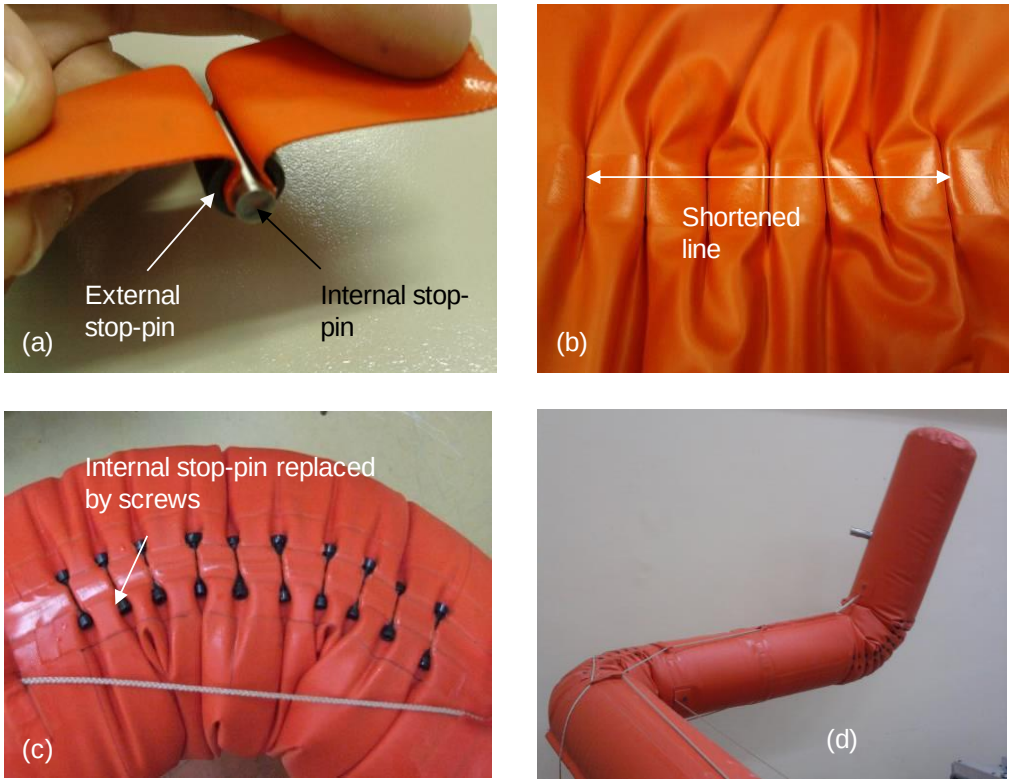

Fig. 8 : Stop-pin principle (a). Joint middle line shortened with stop-pins (b). Joint with stop-pins and screws (c). Two axis prototype made with a PVC coated Polyester fabric (d).

This assumption is confirmed if we consider the stresses in the fabric between two stop-pins (Fig. 9). In the longitudinal direction, the fabric is submitted to the stress σ_T :

$$\sigma_T = \frac{P\pi R^2}{2L_g t_f} \tag{5}$$

Here t_f denotes the thickness of the fabric. The bending torque M applied on the joint creates the stress σ_M :

$$\sigma_M = \frac{4M}{L_g^3 t_f} y \tag{6}$$

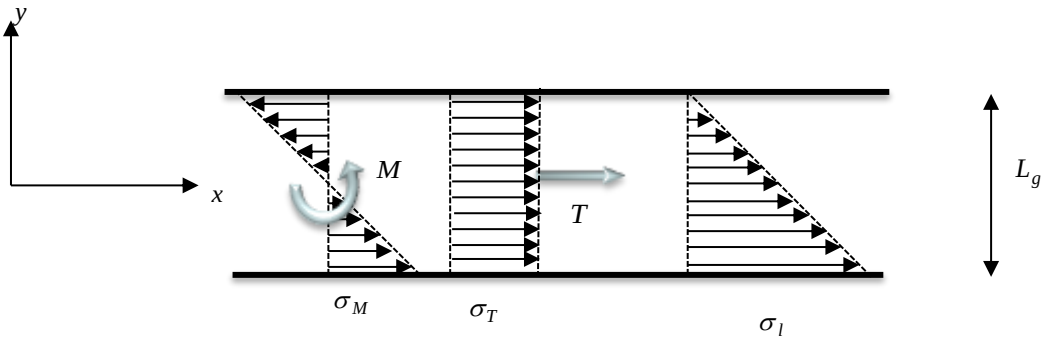

Fig. 9 : Fabric wrap between two stop-pins.

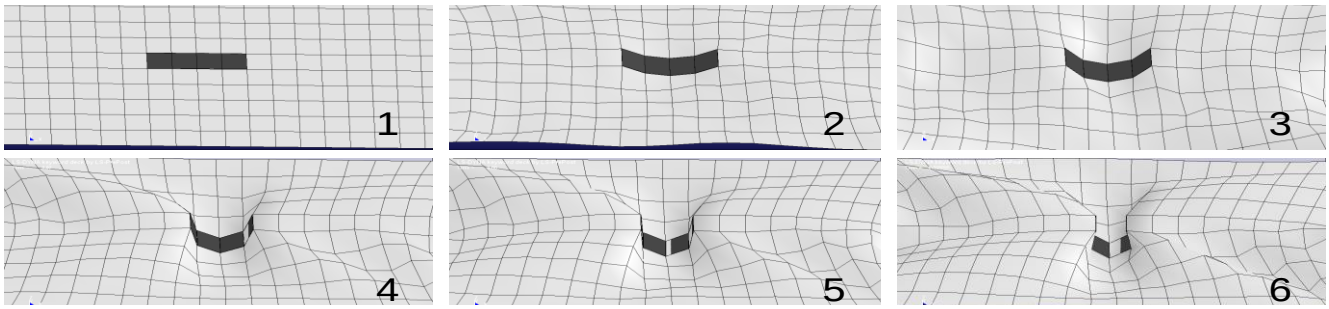

Fig. 10 : Folding of a simulated stop-pin.

Assumed that the fabric can not bear compressive in plane stresses, the joint bends only when:

$$\sigma_l = \sigma_T + \sigma_M = 0 \tag{7}$$

This condition is reached with:

$$y = \frac{L_g}{2} \text{ and } M = \frac{P\pi R^2 L_g}{4} \tag{8}$$

This simple modelling confirms that the torque needed to bend the joint is bigger with long stop-pins. Moreover, best performance should be achieved with zero-length stop-pins. This obviously, does not make physical sense because of the simplicity of this model. Therefore, a more refined model has been developed within the finite element code LS-DYNA in order to evaluate the influence of the stop-pin length.

The simulations consist in inflating the tube at 1.5×10^5 *Pa* and then creating the pleats. The stop-pins are composed of rigid bodies attached to the fabric. The pleats are created when the stop-pins get curved (Fig. 10).

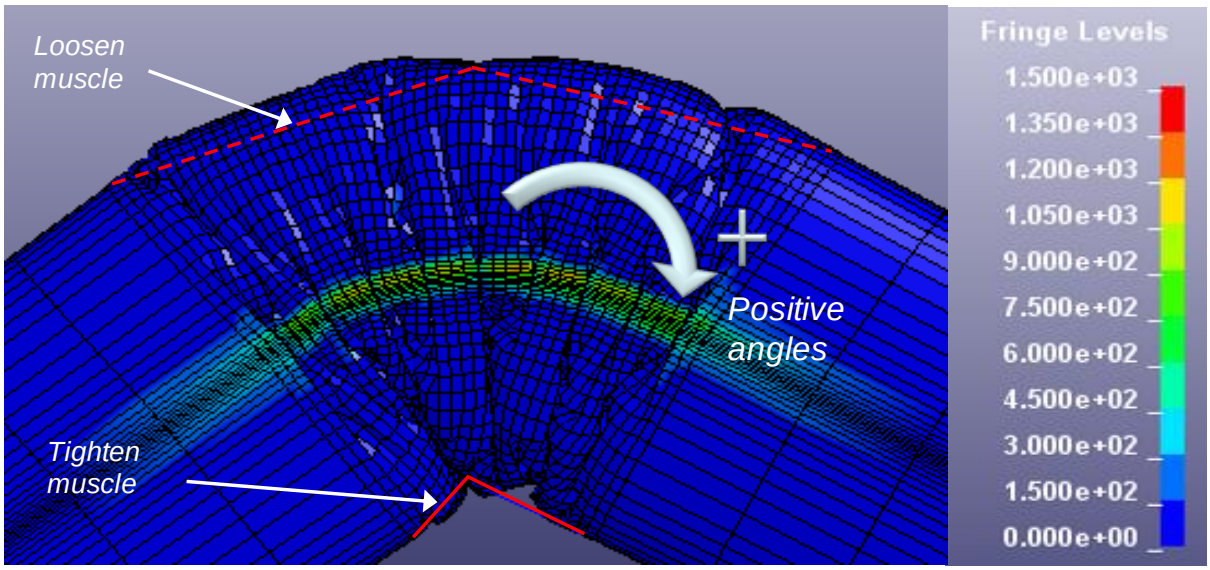

Fig. 11 : Von Mises stress (*MPa*) for a 13.5*mm* stop-pin joint.

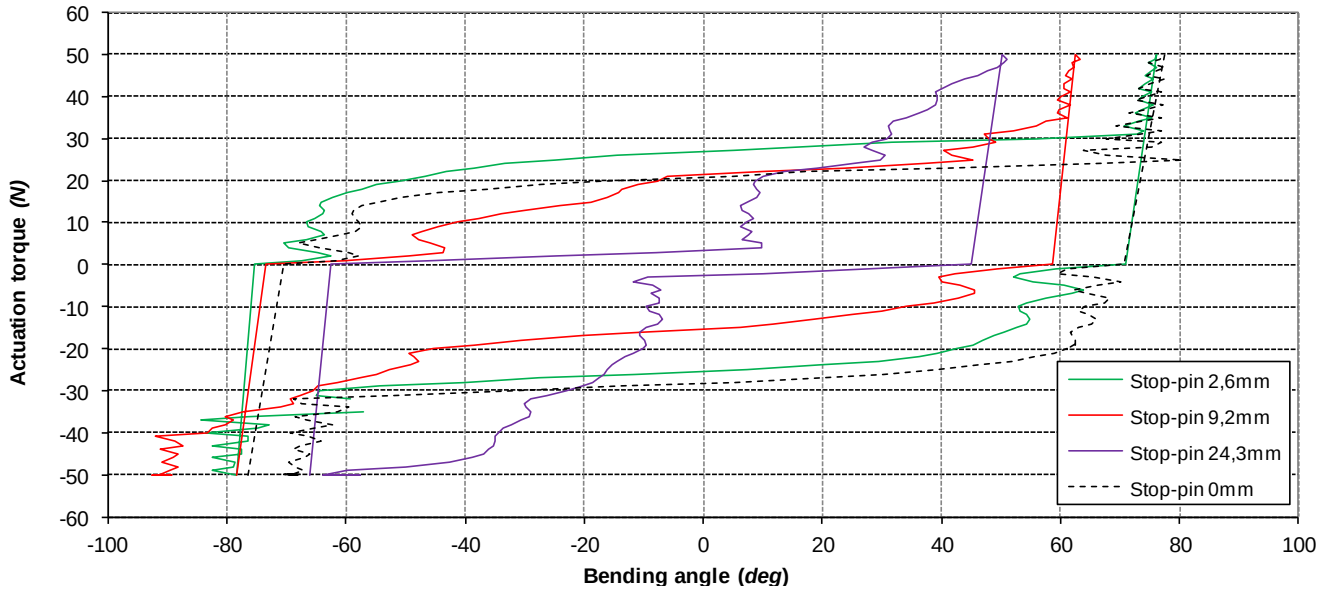

Fig. 12 : Significant responses of stop-pin based joints to a full bending cycle in simulation.

When the middle line is shortened, the fabric between the stop-pins is stressed (Fig. 11). The bending forces are applied by muscle elements located on the sides of the joint (see

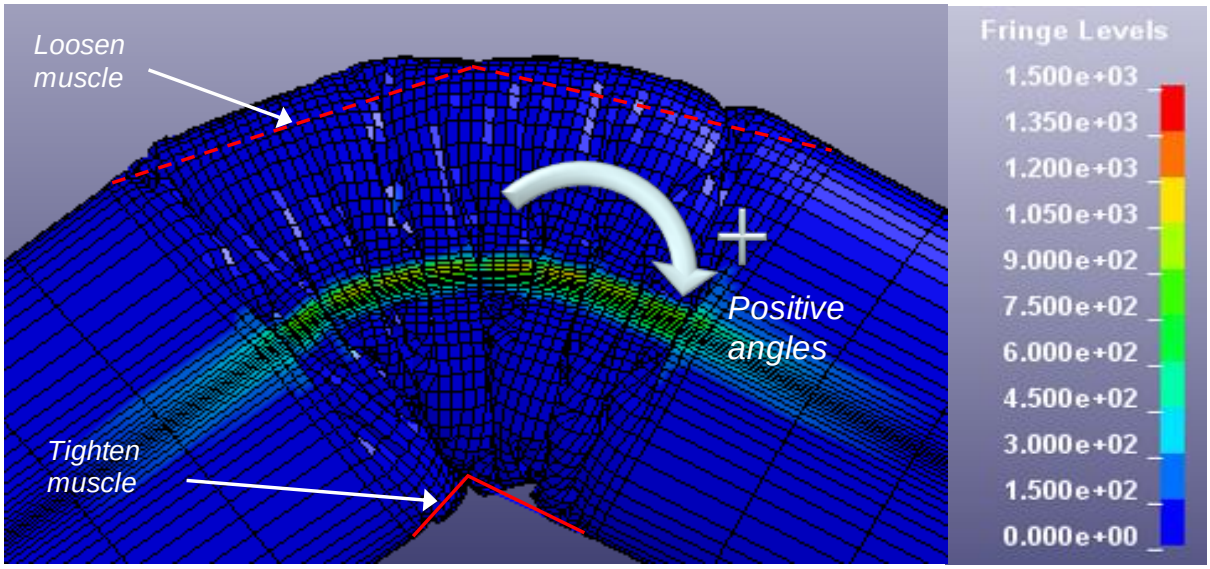

Fig. 11). During the simulation, the antagonist muscles are alternately tighten and loosen in order to bend the joint in positive and negative angles. This simulation is repeated with seven different stop-pins lengths; from 0 to 24.3 *mm*. For clarity, only 4 significant curves are displayed in Fig. 12. The actuation torque is calculated as the sum of the muscles tensions, counted positively for the muscle that produces positive angles and negatively for the other, multiplied by the cylinder radius.

The curves show a hysteresis phenomenon that has been also experimentally pointed out by Schmidt and Newman [28] and Voisembert *et al.* [29], and is called the damping moment. Several studies [9, 28, 30, 31] aim at measuring accurately this resisting force in space-suit joints in order to prepare extravehicular mission.

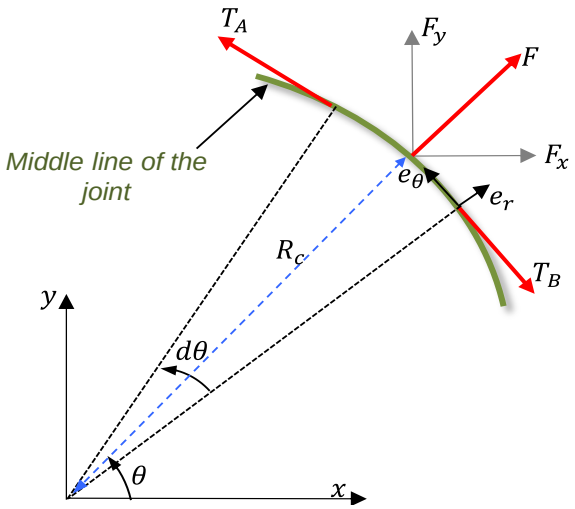

Fig. 13 : Visualisation of the tensions applied on the middle line

It is commonly assumed that the hysteretic behavior of an inflated joint is due to the friction of the fabric fibers. But the numerical simulations show that even without friction modeled, this phenomenon exists. The physical cause of this hysteresis is still under investigation.

We can also observe that for most curves, there is a threshold which represents a minimum effort to apply in order to bend the joint. For short stop-pins, when the bending torque is superior to this threshold, the joint bends with almost no additional effort. The simulations show that a zero-length stop-pin does not provide better performances. The ideal length of the stop-pins is a trade-off because the fabric wrap must be wide enough to bear the tension and thin enough to reduce the minimum bending torque. We propose another solution that overcomes this paradox in the next part.

3.2.2 Wire-based solution

The problem of stop-pin-based solution is that the tension is bear by the fabric itself, and then it must be wide to resist it. If the tension is bear by a wire, the problem is solved. As described in the following paragraph, the wire can not only be bound to the fabric at the extremities of the joint. In fact, when the joint is bent, the shortened middle lines are also submitted to a transverse effort. If we consider a dl length portion of wire, the static equilibrium (Fig. 13) is then expressed as follows:

$$\overrightarrow{T_A} + \overrightarrow{T_B} + F_x\vec{x} + F_y\vec{y} = \vec{0} \tag{9}$$

F_x and F_y denote the components of F , the action of the fabric on the middle line. When $d\theta$ (Fig. 13) is small, we can make the following approximation:

$$\begin{aligned} F_x &= T\left(\sin(\theta + d\theta) - \sin(\theta)\right) \approx T\cos(\theta)d\theta \\ F_y &= -T\left(\cos(\theta + d\theta) - \cos(\theta)\right) \approx T\sin(\theta)d\theta \end{aligned} \tag{10}$$

$d\theta$ can be expressed with the local curvature radius $R_c(\theta)$ and dl:

$$d\theta = \frac{dl}{R_c(\theta)} \tag{11}$$

Therefore:

$$\vec{F} = \frac{T}{R_c(\theta)} dl \vec{e_r} \tag{12}$$

which gives:

$$\sigma_t = \frac{T}{R_c(\theta)} \tag{13}$$

The fabric applies also the lineal transverse tension σ_t on the middle line.

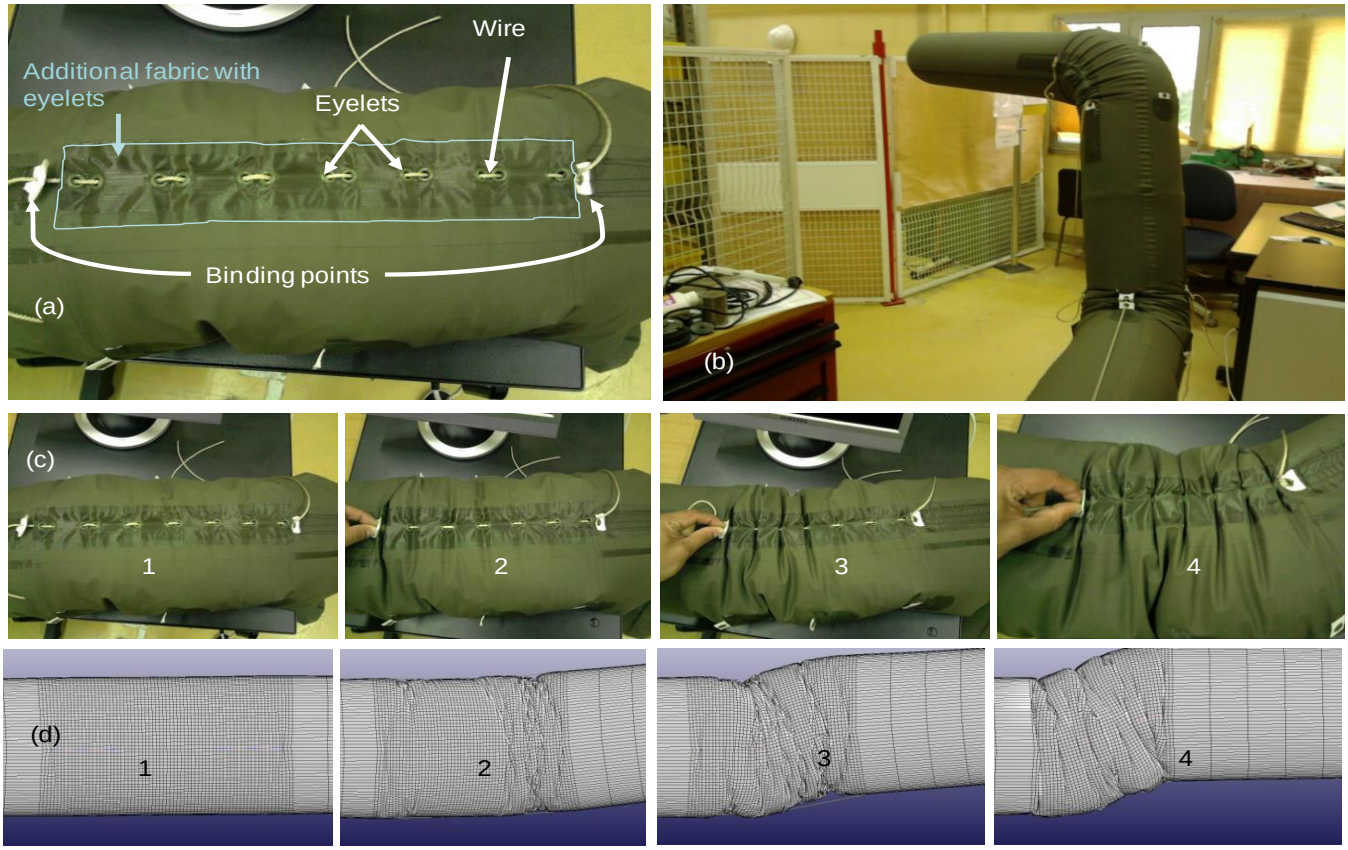

Fig. 14 : Middle line of a joint with a loosen wire (a). Prototype with two wire-based joints (b). Shortening of the middle line of the joint (c). Simulated shortening of the middle line thanks to muscle elements (d).

As a consequence, the wire must be bound at its extremities in order to bear the longitudinal tension but also all the way down the middle line in order to support the transverse tension.

Therefore, the wire is inserted through intermediate eyelets and bound to the final eyelets (Fig. 14a). We have tested this structure and it works on prototypes (Fig. 14b). We have also simulated its behavior (Fig. 14d) in order to compare with the previous design. The wire is modeled by springs and muscles elements.

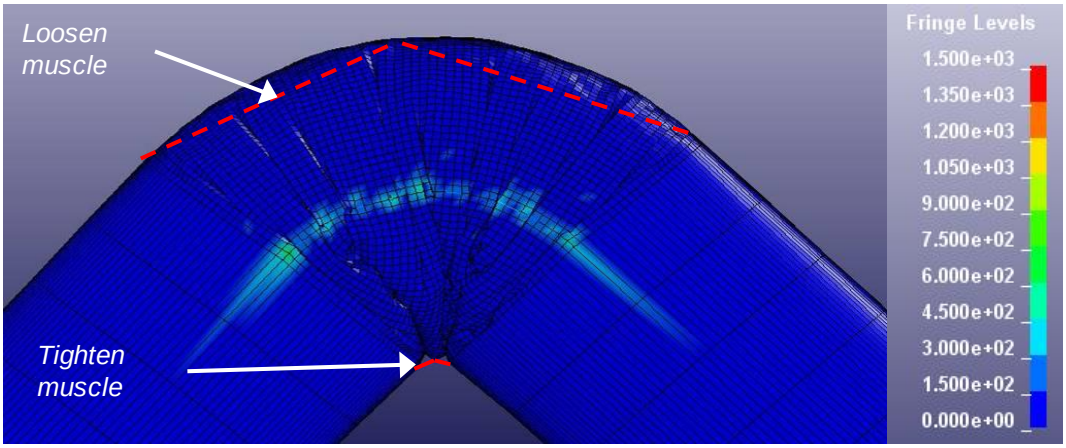

Fig. 15 : Von Mises stress (*MPa*) in the wire based joint.

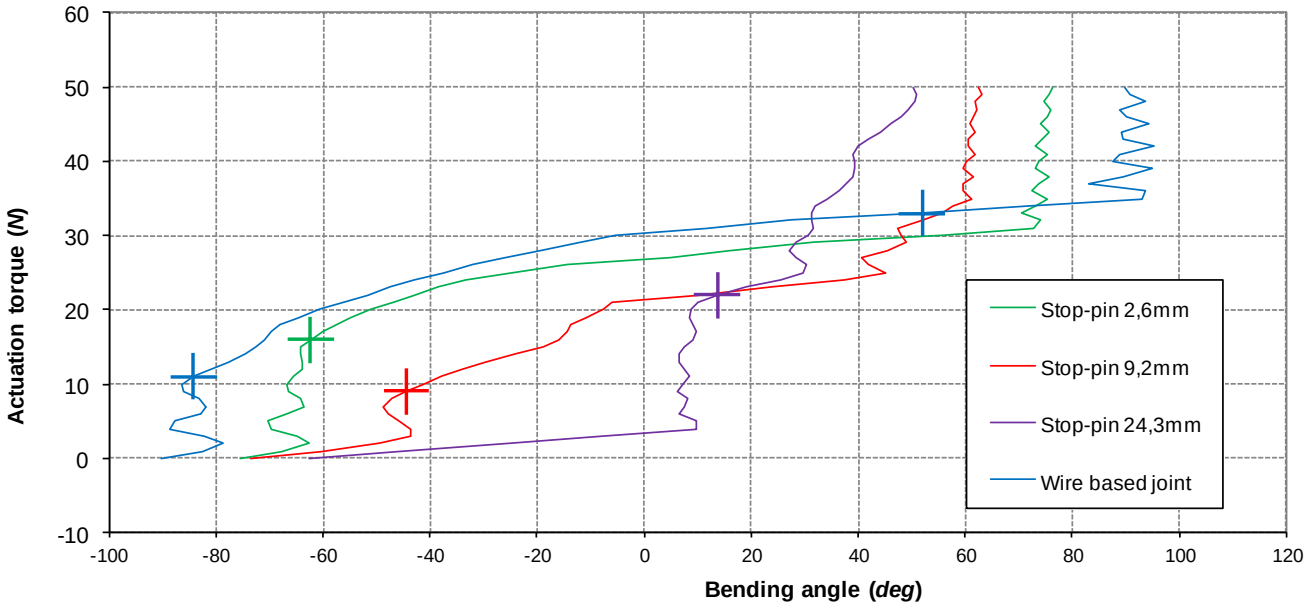

Fig. 16: Significant responses of stop-pin and wire based joints to a half bending cycle in simulation.

When the tube is inflated, the muscles retract and the middle line of the joint is shortened. As the wire supports the longitudinal tension, we can see in Fig. 15 that the fabric in the middle line is not stressed as with the stop-pins.

As a consequence, the wire reduces the risk of fabric tearing. We have also submitted the wire based joint to the same bending cycle as the stop-pin based joint. For cleaner figures, only the half bending cycle is displayed in Fig. 16.

3.2.3 Comparison of the design and friction impact

In order to compare the designs, the actuation threshold and the maximal amplitude are displayed in Fig. 17 for each stop-pin length and for the wire based joint.

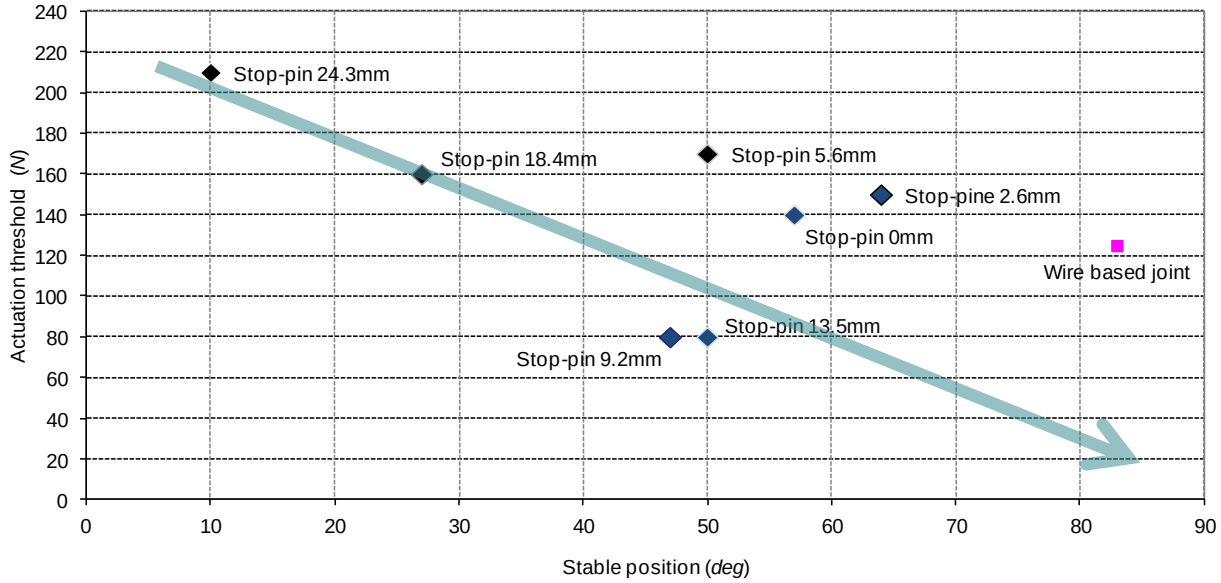

Fig. 17: Comparative evaluation of stop-pin and wire based joint performances.

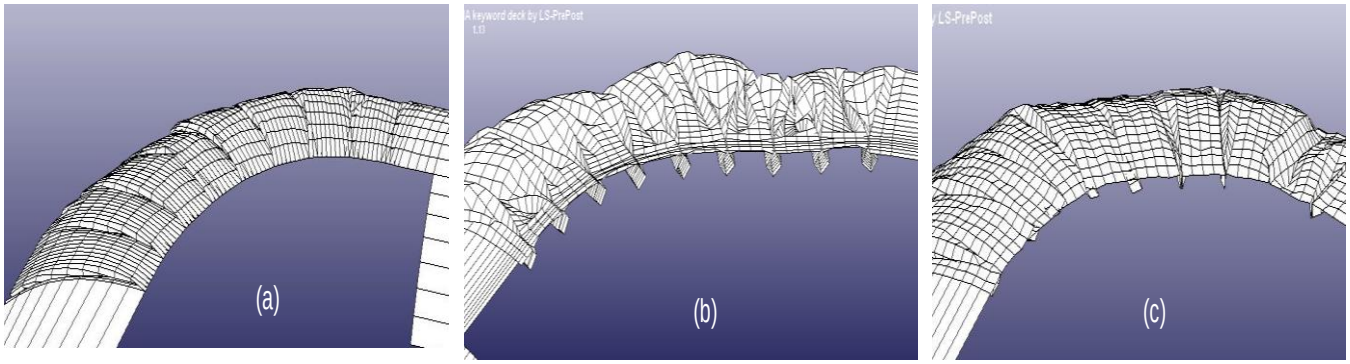

Fig. 18: Flat folds (a). Folds generated by stop-pins (b). Folds generated by the wire (c).

We can see that the wire-based joint has the widest amplitude and an actuation threshold similar to the best stop-pin based joint. Actually, using a wire instead of stop-pins to restrain the middle line is the better solution because it separates the problem of tightness from the problem of bearing concentrated tensions. The assembly precision is also improved because the cable is integrated on the planar fabric before the folds are created. Moreover, pulling the wire is a great deal easier than placing the stop-pins one by one on the fabric.

When tested with and without friction, it appears that friction reduces the joint maximal pitch angle. Nevertheless, this effect represents only 10 % of the pitch angle for stop-pin based joints and 2 % for the wire based joints (see Fig. 19). The previous designs presented in [32] are more impacted (reduction by 70% of the maximum pitch angle) because the folds are in a flat

configuration in which auto-contacts appears near the middle line with shear displacements (see Fig. 18). With the new designs the folds are not constrained and contacts are limited.

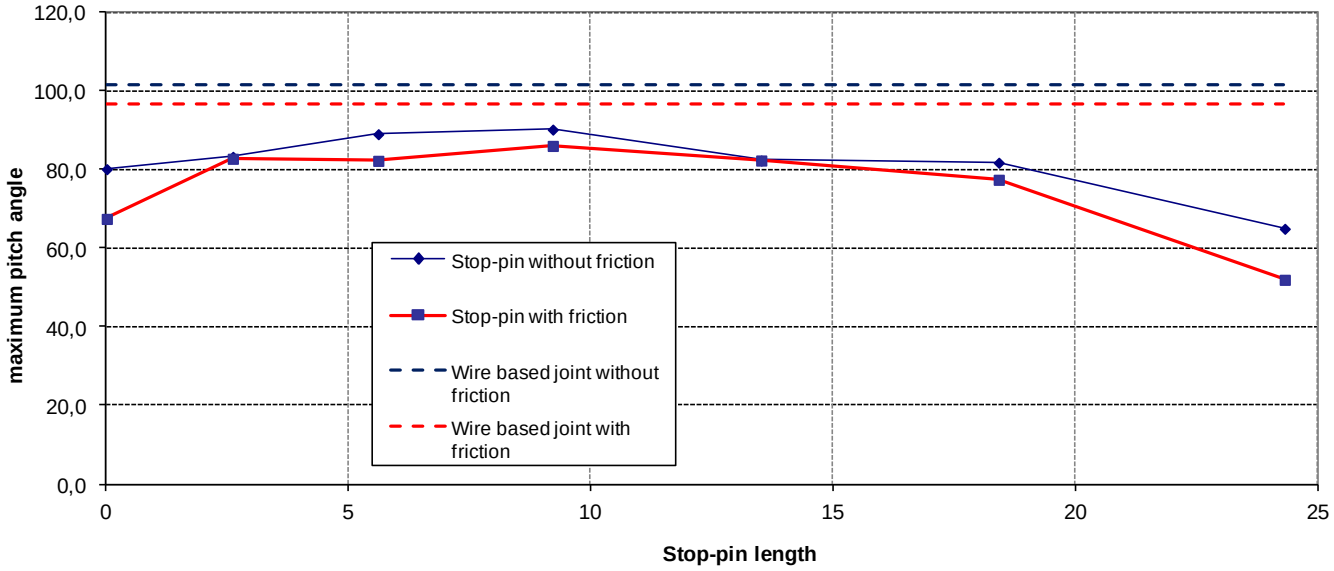

Fig. 19: Friction impact on the maximum pitch angle.

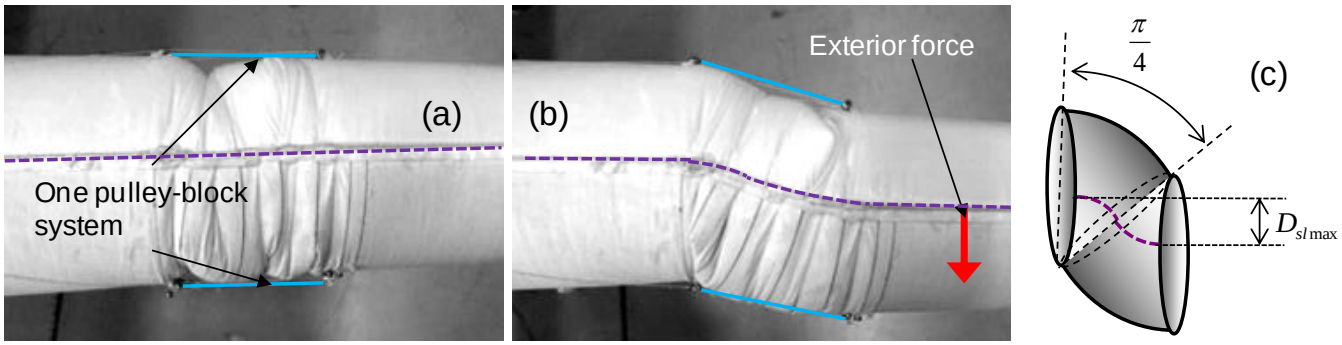

Fig. 20 : Inflatable joint affected by an exterior force .

4 Actuation system

The actuation system must meet the specifications cited in Table 2. In order to add minimum weight, we propose a tendon based system with actuators at the base of the arm [33]. The inflatable joints described in the previous section are basically planar continuously deformable sections.

Table 2: Actuation system specifications

Functions	Requirement	Criteria

Motion	Quasi-static	Quick stop oscillations amplitude < cylinder radius
	Ability to carry loads	Payload/proper weight ≥100%
Kinematics	Full control of every DOF of a joint	Positioning precision < 5%
Coupling	Independent control of the joints	Geometrical motion coupling <1%
Weight	Not adding critical weight	Lineal mass/lineal mass of the arm < 10%

When actuated by tendons, it is possible to control the orientation of the end section, *i.e.* the joint angle [34]. Nevertheless, the curvature can be changed by exterior forces with no possibility for the tendons to counter this effect (Fig. 20). We have called this a dislocation. For an inflatable joint, a dislocation is a non-toroïdal shape that keeps the volume constant. It can be characterized by the lateral displacement, D_{sl}, of the middle line (see Fig. 20c) and the maximal value is given by:

$$D_{slmax} = 2Rsin\left(\frac{\pi}{4}\right) = R\sqrt{2} \qquad (14)$$

In [33] we have proposed and validated an actuation system based on pulley blocks that permits to control the bending angle *and the shape* of a planar continuously deformable inflatable joint.

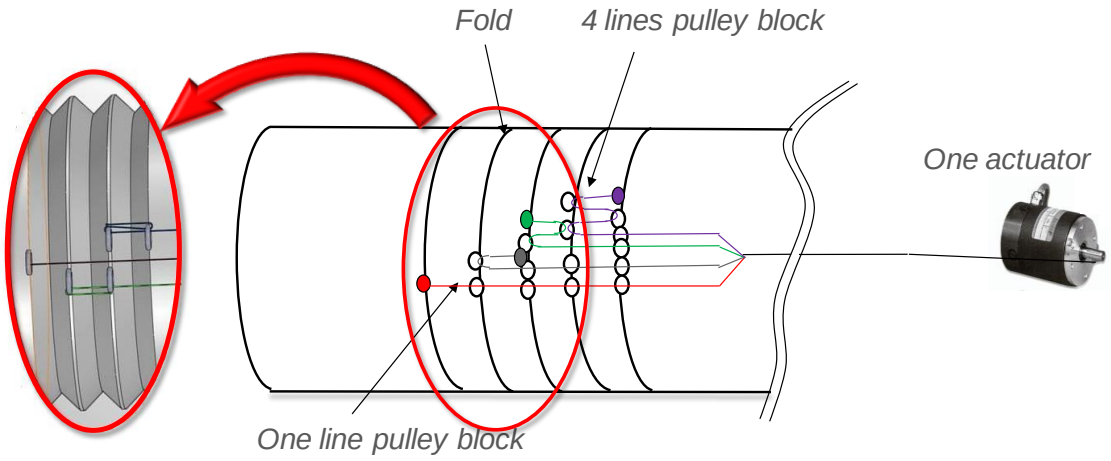

Fig. 21: Pulley block system forcing the joint to keep a toroïdal shape

Provided that the pulley blocks are evenly placed and that every pulley block counts one more line than the next pulley (Fig. 21), the joint is forced to keep a toroïdal shape and the curvature is constant. For more details on the demonstration, see [33].

In order to minimize the mass of the actuation system, we propose to guide the lines in the pulley blocks through simple rings. This method saves the mass of bearing pulleys but poses the problem of friction in the actuation system.

First we have assumed that there should be as many pulley blocks as folds to fully actuate a joint. For a high number of folds this assumption leads to use a high number of pulley blocks, which multiplies the sources of friction.

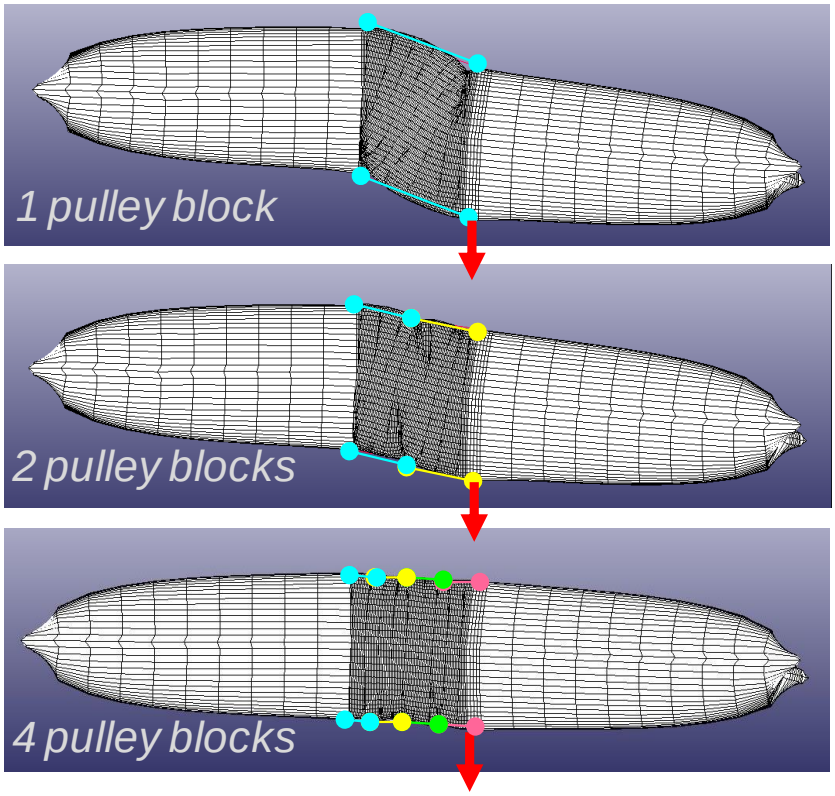

Fig. 22: Simulated joints submitted to dislocations pulley blocks systems

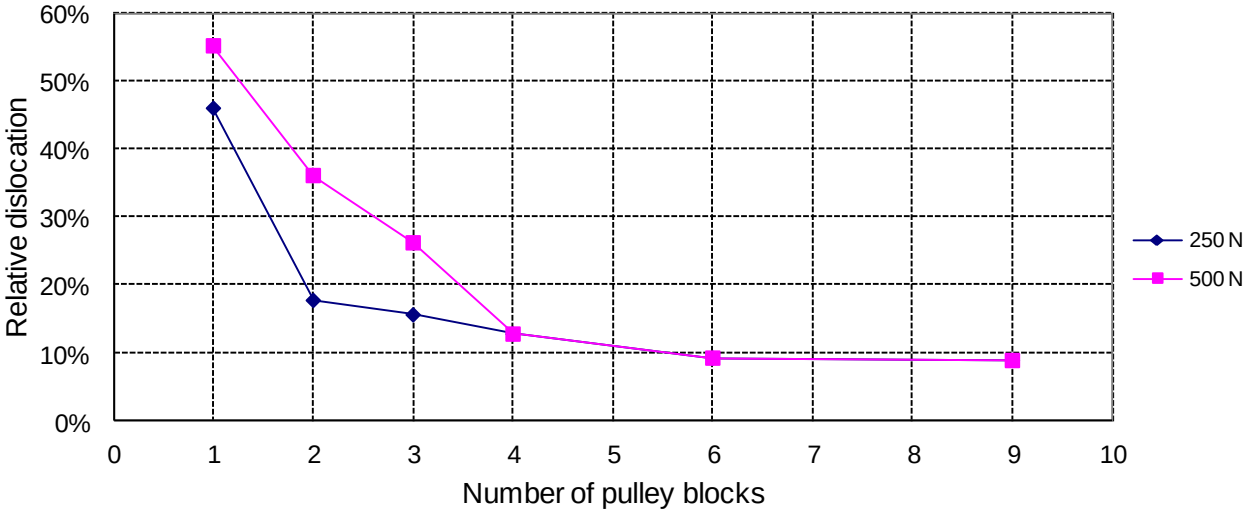

Fig. 23: Relative dislocation with different loads and number of pulley block

In order to define to which extent the joint can be under actuated to reduce friction, we simulate a 90° joint with 9 folds and 1 to 9 pulley blocks (see Fig. 22b) and apply an exterior force. We repeat this simulation with two lateral forces.

The relative dislocations is calculated by dividing the simulated dislocation by the theoretical maximal dislocation. The results are displayed in Fig. 23.

We can observe that having the same number of pulley blocks as of folds is not necessary. Four pulleys are enough to limit the dislocations of a 90° inflatable joint to 13% of the maximal dislocation.

5 Conclusion and future work

In this work, the design of a novel inflatable long-range arm is proposed. This low cost robot, gives new perspectives on several applications as maintenance in critical installation or safe human interaction. Joints of this original design are based on the principle of toroïdal bending at constant volume, which provides low actuation torques.

The comparison of a thin-wall beam with the performances of cutting-edge robots shows that an inflatable long range robot would answer the problem of deflection under gravity. Nevertheless, the deformations of the joints could be more significant than the structural deformations of the links. In future works we will analyze and model the mechanical behavior of the joint and define which could be the real performances of a long range inflatable robot.

This kind of joint is preferred to section-restriction joints because of its higher pitch angle and better torsion stiffness. Two manufacturing procedures for the inflatable joints with a tight coated fabric have been proposed and compared thanks to experimentation and finite element based simulations (LS-DYNA software). One is based on a stop-pin assembly, the other is based on a wire, and both purposes are to shorten the middle line of the joint without drilling the tight coat. The simulations show that both designs present a hysteretic behavior.

Hysteresis is a well known problem for these inflatable joints but is assumed to be caused by friction in the fabric. As a resisting force appears in the simulations, even without friction modeled, we can affirm that this phenomenon is not due to friction. It remains to investigate whether it is caused by “numerical damping”, necessary to calculation stability, or by physical causes other than friction.

The comparative evaluation also shows that the wire-based joint has similar damping moment, and better pitch angle than the stop-pin based joint. Manufacturing experimentations have shown that the wire is easier to manipulate than the stop-pins and reduces the risks of fabric tearing. Nevertheless, even with a wire, the simulated damping moment is high and could be a problem for the tensile actuation system. Therefore, the damping moment will be investigated in order to better understand its origin and reduce its value.

Within a robotic application project, we have developed and numerically evaluated an actuation system based on pulley blocks. It reduces the dislocations, typical of continuously deformable joints, and keeps the curvature constant. As the pulley blocks are a great source of friction for the tendons, we have tested in simulation different numbers of pulley blocks and

determined that a number of 4 is sufficient to reduce significantly the dislocations. In future works we will also test this assessment on prototypes.

The next development step will be to motorize the actuation system and define the control system.

6 References

[1] D. Trivedi, D. Dienno, and C. D. Rahn, "Optimal, Model-Based Design of Soft Robotic Manipulators," *ASME Journal of Mechanical Design,* vol. 130, pp. 14021-9, 2008.
[2] N. Salomonski, M. Shoham, and G. Grossman, "Light robot arm based on inflatable structure," *Annals of the ClRP,* vol. 44, 1995.
[3] Y. Koren and Y. Weinstein, "Inflatable Structure," USA Patent, 1991.
[4] R. Baldur and W. Blach, *Inflatable manipulator*: Society of Manufacturing Engineers, 1985.
[5] S. Sanan, J. B. Moidel, and C. G. Atkeson, "Robots with Inflatable Links," presented at the International Conference on Intelligent Robots and Systems, St. Louis, USA, 2009.
[6] S. Sanan, "Soft Robots for Safe Physical Human Interaction," The Robotic Institute, Carnegie Mellon University, Pittsburgh, 2010.
[7] L. Gargiuloa, P. Bayetti, V. Brunoa, J.-C. Hatchressiana, C. Hernandeza, M. Hourya, D. Keller, Jean-Pierre Martinsa, Y. Measson, Y. Perrot, and F. Samaillea, "Operation of an ITER Relevant Inspection Robot on Tore Supra tokamak," *Fusion Engineering and Design*, vol. 84, pp. 220–223, 2009.
[8] D. Keller, J. P. Friconneau, and Y. Perrot, "An ITER Relevant Robot for Remote Handling: on the Road to Operation on Tore Supra," in *Advances in Service Robots*, InTech ed, 2008.
[9] M. H. Jin, J. D. Zhao, H. Y. Hu, L. B. Du, X. H. Gao, T. Q. Li, Y. J. Zhao, and H. Liu, "A Six DOF Passive Robot System for Spacesuit Measurement," presented at the Conference on Advenced Intelligent Mecatronics, Kobe, 2003.
[10] G. C. Tsiatas and J. T. Katsikadelis, "Large Deflection Analysis of Elastic Space Membranes," *International Journal for Numerical Methods in Engineering*, vol. 65, pp. 264–294, 2006.
[11] J. Troufflard, J. M. Cadou, and G. Rio, "Recherche de Forme des Gilets de Sauvetage Gonflables," *Mécanique et Industrie*, vol. 11, pp. 117-122, 2010.
[12] J. Troufflard, J. M. Cadou, and G. Rio, "Simulation Numérique de Recherche de Forme : Application aux Gilets de Sauvetage Gonflables," presented at the Congrès Français de Mécanique, Grenoble, France, 2007.
[13] J. Breukels and W. J. Ockels, "Analysis of Complex Inflatable Structures Using a Multi-Body Dynamics Approach," presented at the Structures, Structural Dynamics, and materials Conference, Schaumburg, IL, USA, 2008.
[14] D. Fokin, N. Lokhande, and L. Fredriksson, "On Airbag Simulation in LS-DYNA with the Use of the Arbitrary Lagrangian-Eulerian Method," presented at the 4th European LS-DYNA Users Conference, Ulm, Germany, 2005.
[15] A. Diaby, "Contribution à l'Etude du Flambement des Structures Gonflables," Ecole doctorale "Mécanique, Thermique et Génie Civil", Faculté des Sciences et Techniques, Nantes, 2005.
[16] W. Davids, "Finite-Element Analysis of Tubular Fabric Beams Including Pressure Effects and Local Fabric Wrinkling," *Finite Elements in Analysis and Design*, vol. 44, pp. 24-33, 2007.
[17] M. R. Barnes, "Form-Finding and Analysis of Prestressed Nets and Membranes," *Computers and Structures*, vol. 30, pp. 685-695, 1988.
[18] T. J. R. Hughes, R. L. Taylor, J. L. Sackman, A. Curnier, and W. Kanoknukulchai, "A Finite Element Method for a Class of Contact-Impact Problems," *Computers Methods in Applied Mechanics And Engineering*, vol. 8, pp. 249-276, 1975.
[19] J. O. Hallquist, "LS-DYNA Theory Manual," LSTC2006.
[20] LSTC, "LS-DYNA Keyword User's Guide," 2007.
[21] J. T. Wang and O. J. Nefske, "A New CAL3D Airbag Inflation Model," *Society of Automotive Engineers Transactions*, 1988.
[22] J. T. Wang, "Dynamic Deployement Simulations of Inflatable Space Structures," presented at the International Conference on Computation of Shell and Spatial Structures, Salsburg, Austria, 2005.
[23] R. L. Comer and S. Levy, "Deflections of an Inflated Circular-Cylindrical Cantilever Beam," *AIAA Journal*, vol. 1, pp. 1652–1655., 1963.
[24] A. Le Van and C. Wielgosz, "Bending and Buckling of Inflatable Beams: Some New Theoretical Results," *Thin-Walled Structures*, vol. 43, pp. 1166-1187, 2005.
[25] C. Wielgosz and J. C. Thomas, "Deflection of Inflatable Fabric Panels at High Pressure," *Thin Walled Structures*, vol. 40, pp. 523-536, 2002.
[26] C. Wielgosz, J. C. Thomas, and A. Le Van, "Mechanics of Inflatable Fabric Beams," presented at the International Conference on Computational & Experimental Engineering and Sciences Honolulu, Hawaii, USA, 2008.
[27] R. Courant, K. Friedrichs, and H. Lewy, "On the Partial Difference Equations of Mathematical Physics," *AEC Computing Facility, New York University*, 1956.
[28] P. B. Schmidt and D. J. Newman, "Modeling Space Suit Mobility: Applications to Design and Operations," presented at the International Conference on Environmental Systems, Orlando, USA, 2001.
[29] S. Voisembert, A. Riwan, N. Mechbal, and A. Barraco, "A Novel Inflatable Robot with Constant Continuous Volume," in *International Conference on Robotics and automation*, Shanghai, China, 2011, pp. 5843 - 5848
[30] P. Schmidt, "An Investigation of Space Suit Mobility With Applications to EVA Operations," Dept. of Aeronautics and Astronautics, Institute of Technology, Massachusetts, 2001.
[31] D. J. Newman, P. B. Schmidt, D. Rahn, N. Badler, and D. Metaxas, "Modeling the Extravehicular Mobility Unit (EMU) Space Suit Physiological Impliacations for Extravehicular Activity (EVA)," presented at the Conference on Environmental Systems, Toulouse, 2000.
[32] S. Voisembert, A. Riwan, and N. Mechbal, "Numerical Evaluation of a New Robotic Manipulator based on Inflatable Joints," presented at the Conference on Automation Science and Engineering, Seoul, 2012.
[33] S. Voisembert, A. Riwan, N. Mechbal, and A. Barraco, "A Novel Inflatable Tendon Driven Manipulator with Constant Volume," in *Mechanisms and Robotics Conference*, Washington, USA, 2011, pp. 1233-1242
[34] I. A. Gravagne and I. D. Walker, "On the Kinematics of Remotely-Actuated Continuum Robots," presented at the International Conference on Robotics and Automation, San Fransisco, USA, 2000.